Response to Reviewer 1 Comments:

Zou et al. corrected the degradation trend of GOME-2A SIF with a pseudo-invariant method, based on a 1 degree x 1 degree calibration region in the Sahara Desert. Unlike previous studies, the correction in this study was conducted at radiance level and daily basis, using a fitted quadratic polynomial function. Then the SIF signal was retrieved using a data-driven algorithm, which was further scaled to monthly average with a PAR-based upscaling model. The global trend of the corrected SIF data was also compared with several existing SIF/GPP/NDVI products. The study is overall nicely conducted.

Thank you for your thorough and insightful review of our manuscript. We appreciate the time and effort you invested in providing valuable feedback. We have carefully considered each of your comments and suggestions. Please find the point-by-point responses below.

Major comment 1: Benchmarks used for trend evaluation: The authors employed MODIS NDVI and a number of GPP datasets from MODIS and model simulations, to evaluate the trend of TCSIF. However, MODIS NDVI has a known saturation effect, which would especially influence the evaluation of annual maximum (Fig. 11). MODIS GPP and TRENDY GPP are also known to have issues with their trends (Anav et al., 2015, https://doi.org/10.1002/2015RG000483). I would not trust the evaluation against these datasets.

Response: Thanks for this comment. We agree that the trend of GPP and NDVI cannot serve as benchmarks for the time series of SIF, in this study, they can only used for indirect comparison. We used the annual maximum to derive trends when the vegetation is most vigorous, while NDVI shows its limitation of not being able to catch the trend of GPP compared with SIF.

These indirect validations were moved to the discussion part (Sec.5.3 and Sec. 5.4). Instead, we added a two-step validation for both the corrected radiance spectra (in Sec. 4.1) and the retrieved SIF (in Sec. 4.3) of the revised manuscript.

Radiance spectra obtained from GOME-2C serve as a benchmark for the radiance spectra. Being a sensor that measures the same bands with the same spectral resolution as GOME-2A, GOME-2C has a later launching time in November 2018. Thus, measurements at the initial launch stage of GOME-2C can be taken as accurate values that are not affected by degradation. The pseudo-invariant calibration method was verified by validating temporal corrected radiance in Sec. 4.1 **(Line 256)**:

4.1 Correction of GOME-2A sensor degradation

The temporally corrected GOME-2A NIR radiance was validated using GOME-2C radiance spectra (Figure 4). For the corrected GOME-2A radiance, the scatter plot shows that the majority of points are

concentrated near the 1:1 line (Figure 4a). The slight positive offset of the linear regression may be caused by the lower orbit height of GOME-2C (817 km) than GOME-2A (827 km), which results in less atmospheric absorption in GOME-2C. The difference between the two products followed a Gaussian distribution with a small mean value of 1.85 mW m^{-2} sr^{-1} nm^{-1}, which is 2.3% of the mean GOME-2A radiance (Figure 4b). On the contrary, the mean deviation without temporal correction is 15.16W m^{-2} sr^{-1} nm^{-1} (Figure 4d).
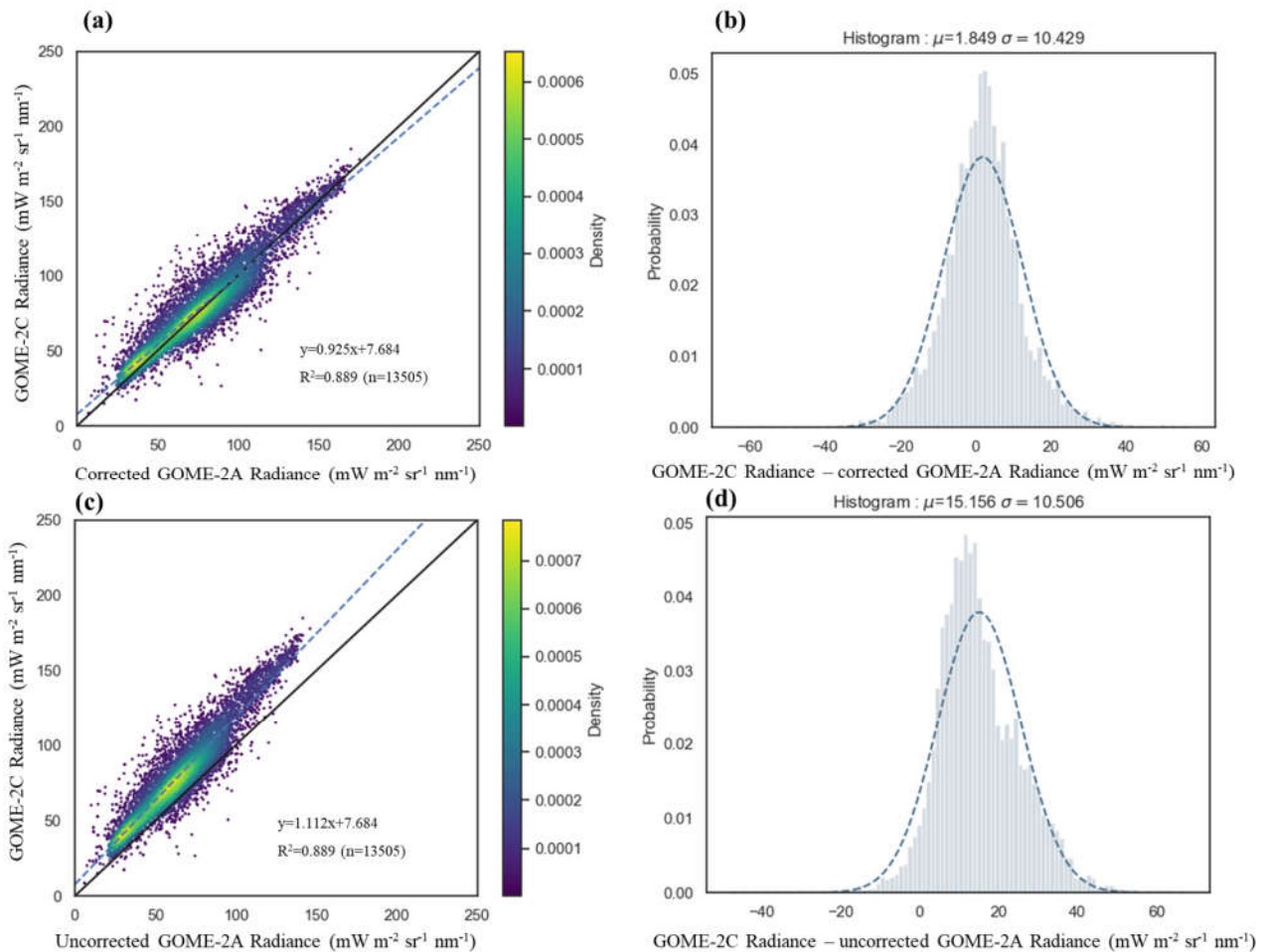
Figure 4 Comparison between GOME-2A and GOME-2C NIR radiance after (a,b) and before (c,d) the temporal correction on 1 July 2019. The histogram of difference for GOME-C NIR radiance minus the corrected and uncorrected GOME-2A NIR radiance was shown in (b) and (d), respectively. Spatially matched pixels with cloud fraction of lower than 0.3 and SZA of lower than 70° were selected.

Besides, TCSIF has been validated in Sec. 4.3 **(Line 295)** with OCO-2 SIF and TROPOMI SIF, the results are shown below:

4.3 Spatial distribution of the TCSIF dataset

OCO-2 SIF and TROPOMI SIF were also involved in the validation of TCSIF (Figure 7 e,f). To avoid discrepancies in wavelength and the overpassing time, the day-length corrected 740 nm provided by OCO-2

SIF, TROPOMI SIF, and TCSIF were compared. The spatially matched points were selected. TCSIF versus OCO-2 SIF and TCSIF versus TROPOMI SIF comparisons were conducted in July 2019 and July 2021, respectively. Both comparisons show high consistency with $R^2 > 0.65$, and the linear regression results are close to the 1:1 line.
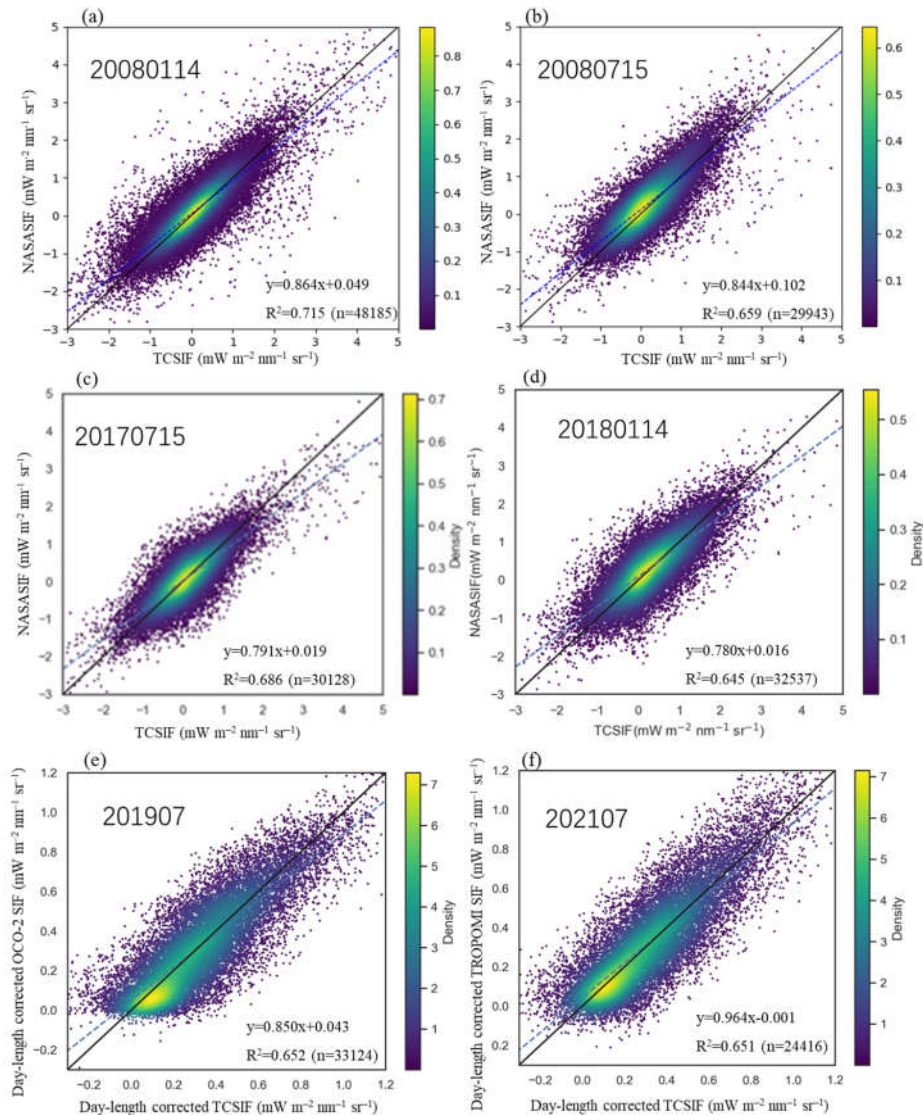
Figure 7. Comparison of TCSIF vs. NASA SIF on 14 January (a) and 15 July (b) in the year 2008, 15 July 2017 (c), and 14 January 2018 (d). **Comparison of TCSIF versus OCO-2 in July 2019 (e) and TCSIF versus TROPOMI SIF in July 2021 (f).** The comparison was made based on the level 2 product. Co-located pixels over land with a cloud fraction < 0.3 have been selected. The color of the scatter points represents the density of the points. The blue dotted line and the black solid line represent the line fitted based on the scatter points and the 1:1 line, respectively.

Besides, temporal comparisons were made between TCSIF and OCO-2 by demonstrating the trend map (detailed in **minor comment 8**) as well as the yearly average curve (detailed in **minor comment 9**). The

analysis of the TROPOMI time series is not shown because the TROPOMI dataset only contains gridded data between 2018.4 and 2021.3, which means that there are only two full years of data in 2019 and 2020. Therefore, TROPOMI SIF is currently not able to provide accurate temporal trends.

Major comment 2: Pseudo-invariant method and site: The authors employed a pseudo-invariant method and selected a 1 degree x 1 degree non-vegetated region which trend was taken as the temporal degradation in the GOME-2A instrument. It has a strong underlying assumption that the degradation trend is the same for different locations and different radiance levels. It remained to be tested/discussed to what extent this is true.

Response: Thanks for this comment. The influence of BRDF and atmospheric conditions limits the selection of diversified pseudo-invariant sample points. Only bright, stable, and homogenous sites can be chosen for the calibration of GOME-2A, thus the desert surface is the most ideal choice. Since the decay function fitted by only one site may not be convincing enough, we added three other commonly used pseudo-invariant calibration sites (PICS). The results show high consistency between degradation functions fitted by those PICS. We have added relative analysis to the discussion part of the revised manuscript as follows:

==Line 346:==

5.1 Degradation at different locations and wavelengths

In this study, only one calibration site (Libya 4) was used for the fitting of the degradation function. The results may be different for different sites. Previous studies have compiled 20 pseudo-invariant calibration sites(PICS) for instrument calibration (Cosnefroy et al., 1996; Bacour et al., 2019). We have involved three other commonly used sites, and the relative information is shown in Table 3.

Table 3 Four pseudo-invariant calibration sites (PICS) and related information

Site name	location	NIR reflectance	mean variation	spatial	temporal variation
Libya 4	(23.00° E, 29.00° N)	55.3 %–60.6 %	0.29 %		0.81 %
Algeria 3	(7.66° E, 30.33° N)	49.2 %–59.3 %	0.94%		1.20%
Mauritania 1	(9.30° W, 19.40° N)	48.3 %–65.6 %	3.48%		2.25%
Libya 1	(13.35° E, 24.42° N)	50.2 %–66.2 %	2.51%		2.25%

Among the four PICS, Libya 4 was shown to be the most ideal site for the calibration, which is bright (the near-infrared [NIR] reflectance is high, at 55.3 %–60.6 %), most homogeneous (with mean spatial variation = 0.29 %), and most stable (with very low temporal variation = 0.81 %). On the other hand, similar

interannual decline trends are given by the four PICS (Figure 12 a). The NIR reflectance of Libya 4, Algeria 3, Mauritania 1, and Libya 1 declined by 16.21%, 17.57%, 17.20%, and 16.38% from 2007 to 2021, respectively. Therefore, it is reliable to fit the degradation of GOME-2A using Libya 4 site only.
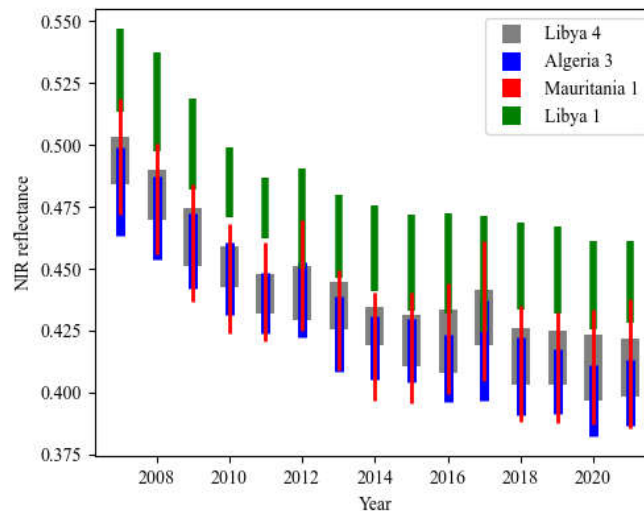
Figure 12. Instrument degradation at four different calibration sites. The center of each bar shows the yearly average, while the length of the bars represents twice the yearly standard deviation.

Results from the four PICS show that there is no significantly greater or smaller degradation at the Libya 1 site although the radiance level is higher than the other three sites.

Various targets with very high or very low radiance levels, such as snow or water bodies, were not selected in this study. This is limited by the temporal stability requirement of choosing the pseudo-invariant calibration site. Regarding this, we stated in the discussion that the radiance range of the Libya 4 site almost covers the radiance levels of vegetation. Thus, the degradation function fitted by these sites be considered effective for vegetation targets. The relative statement is as below. Besides, the sentence *"A wide range of radiance is essential for ensuring the representativeness of the temporal correction function, since the signal-to-noise ratio may differ across different radiance levels."* in line 376 of the previous manuscript was not accurate, and the "signal-to-noise ratio" was changed to "degradation" in the revised manuscript.

==Line 375:==

5.2 Uncertainty in the temporal correction method

A wide range of radiance is essential for ensuring the representativeness of the temporal correction function, since the **degradation** may differ across different radiance levels. Although the pseudo-invariant sampling region selected in this study has a small spatial extent it has a large radiance range (48–284 mW m^{-2} sr^{-1} nm^{-1}), which almost covers that of the main vegetation areas at the near-infrared band (Figure 14); only the lowest value of vegetation radiance (24 mW m^{-2} sr^{-1} nm^{-1}) is not covered. Since the temporal

invariance feature is required for the calibration site, it leaves a few optional samples to choose from. The representativeness of samples may have an impact on the correction coefficient.

Another limitation is that we only indirectly verify the reliability of the interannual trend of TCSIF when using several long-term remote sensing products, such as GPP, NDVI, and other SIF products. Direct validation data, such as field measurements, were not used to prove the accuracy of our results. In this respect, the huge discrepancy in scale between the satellite SIF products (0.5°) and ground observations (<100 km^2) is one of the major obstacles. In fact, moreover, to our best knowledge, there is no decade-long in-situ SIF validation dataset available that is sufficiently reliable for such a direct validation, and the methodology of directly verifying satellite SIF based on in-situ measurements is still imperfect (Parazoo et al., 2019). The accuracy of TCSIF products needs to be verified via future applications.
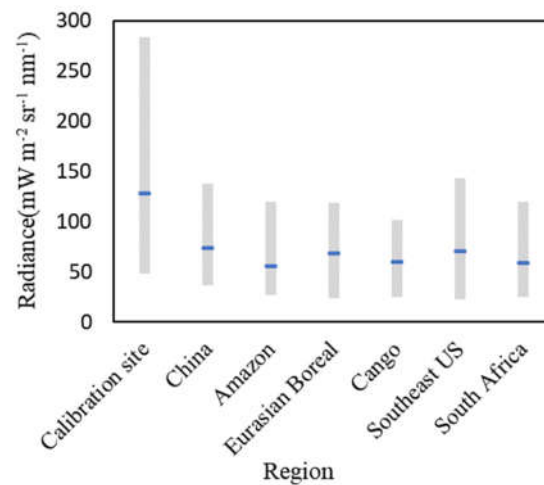
Figure 14. Range of radiance at the near-infrared band at the calibration site and in the six main vegetated areas. The gray bars and blue lines are the range and mean of the datasets, respectively.

For example, in Fig. 9, the authors showed the difference in the temporal trend with and without the correction, which is basically the degradation trend. There are large spatial variabilities in the degradation trend.

Response: Thanks for the comment. It's true that we can see large spatial variabilities in the degradation trend between NASA SIF and TCSIF in Fig.9. However, there will be uncertainties if we take the difference between NASA SIF (without correction) and TCSIF (with correction) in Fig. 9 as the degradation trend of GOME-2. Firstly, different fitting windows and data-driven models were used for SIF retrieval by NASA SIF and TCSIF, which caused inevitable differences in the spatial distribution between the two products. Secondly, the zero-offset corrections were conducted for both of the products to get the final global SIF map. The zero-offset correction deals with the systematic error of the SIF retrieval variant with latitude and radiance. The correction coefficient changes with latitude, radiance, and time, so there may be great uncertainty if taking the difference in the growth trend of the two products as a recession trend.

Minor comment 1: Line 13: This is not accurate. As the authors cited in Table 2, there have been several efforts for correcting the temporal degradation of GOME-2A SIF.

Response: Thanks for this comment. Here, we want to emphasize that the existing GOME-2 temporal correction SIF products still have unfixed problems. For example, LTSIFc is directly corrected based on the 0.5° gridded global SIF products, but the degradation of the sensor is not linearly transmitted to the degradation of SIF products. Meanwhile, SIFTER gives quarterly correction factors, leading to large annual fluctuations. Therefore, it is very necessary to solve the temporal degradation problem from the radiance source. The sentence has been revised as follows:

However, serious temporal degradation of the GOME-2A instrument is a problem, **and for now, there is a lack of time-consistent GOME-2A SIF products that meet the needs of temporal trend analysis.**

Minor comment 2: Line 19: By "weather conditions", I assume it referred to only light conditions?

Response: Thanks for this comment, in this manuscript, by "weather conditions" we mean that the variance of atmospheric conditions (for example, the atmospheric scatter and the effect of clouds) during the day was considered, not only light conditions caused by solar angles, by using PAR instead of cos(SZA). Using this approach, it's more accurate to upscale instantaneous clear-day SIF to the daily average.

Minor comment 3: Line 88: MCD43C4 is provided at daily resolution.

Response: We apologize for the mistake, MCD43C4 is daily data synthesized over 16 days, sorry for confusing the two concepts in the previous version of the manuscript. The description was revised as follows: The MODIS Version 6.1 Nadir Bidirectional reflectance distribution Adjusted Reflectance (NBAR) product (MCD43C4) (Schaaf et al., 2002) records the surface reflectance at a nadir viewing angle for each pixel at local solar noon. It has a spatial resolution of 0.05° × 0.05° and a **daily** temporal resolution (Schaaf et al., 2002). The MODIS NBAR product is considered stable over long periods of time and was used here to investigate the homogeneity and stability of the calibration site (see Sect. 3.1).

Minor comment 4: Line 112: The authors did not provide the links for the datasets used in this study. For NASA SIF, there is a recent updated version here: https://daac.ornl.gov/SIF-ESDR/guides/MetOpA_GOME2_SIF.html. It is generated with updated GOME-2 Level 1B radiances and irradiances, and I heard that the degradation trend has been largely corrected. If the authors used an older version, I'd suggest comparing with this updated dataset too.

Thanks for this comment. We are already using the latest version of the NASA SIF data. Although this

version of the data uses the latest GOME-2 Level 1b data, as explained in the user guide of the latest NASA SIF product, the data has not yet been analyzed for potential errors caused by instrument degradation trends and therefore, is not recommended for long-term analysis.

We have added the link and the introduction of NASA SIF, as well as other products used in the dataset fraction of the revised manuscript as follows:

Line 113:

Next, we selected four long-term SIF products spanning more than one decade for comparison, including the LT_SIFc*(1995–2018) (Wang et al., 2022), SIFTER v2 (2007–2018) (Schaik et al., 2020), GOSIF (2000–2022) (Li and Xiao, 2019), and GOME-2 SIF products generated by the National Aeronautics and Space Administration (hereon abbreviated as NASA SIF, https://daac.ornl.gov/SIF-ESDR/guides/MetOpA_GOME2_SIF) (2007–2018) (Joiner et al., 2013&2016). The LT_SIFc*(https://doi.org/10.6084/m9.figshare.21546066.v1) is a data fusion product of GOME, SCIAMACHY, and GOME-2, having a spatial resolution of 0.05° and a temporal resolution of 1 month. It dealt with the temporal decay of the instrument based on statistics of SIF signals in the Sahara Desert. The SIFTER v2 product **(https://www.temis.nl/surface/sif.php)** is the point-by-point SIF product retrieved from GOME-2 measurements after applying a time-related correction factor; it was composited to yield a 0.5°, monthly global map in this study. The GOSIF product **(https://globalecology.unh.edu/data/GOSIF.html)** is the spatiotemporal expansion product based on the global neural network model and OCO-2 SIF V8r product, with a spatial resolution of 0.05° and a temporal resolution of 8 days. Apart from the SIF products spanning decades, the OCO-2 SIF product **(https://disc.gsfc.nasa.gov/datasets/OCO2_L2_Lite_SIF_10r/summary)** from 2015 to 2021, **and TROPOMI SIF (ftp://fluo.gps.caltech.edu/data/tropomi/) from 2018 to 2021** are also included here for comparative purposed given its high accuracy and it is being less affected by sensor degradation. All SIF products were resampled to a 0.5°, monthly spatiotemporal resolution and were compared with TCSIF to assess long-term trends in this study. Additionally, we used the NASA GOME-2A level 2 SIF product, which has not been corrected for temporal decay, to verify the spatial distribution of our product. Key information about these SIF products is presented in Table 2.

Minor comment 5: Line 159: The function f should be introduced here.

Response: Thanks for this comment. In section 3, we mainly introduce the method of fitting the time degradation. The specific fitting coefficients are given in section 4. According to your suggestions, we show the form of the temporal-degradation function in section 3 **(Line 166)** and guide the readers in finding the fitting process in the results section **(Line 253).** The modifications are as follows:

https://doi.org/10.5194/essd-2023-329

Line 166:

Thus, a time-dependent correction factor was calculated, and the temporal correction function was assumed to be a second-order polynomial as follows:

$$\text{Dfactor} = a \cdot NOD^2 + b \cdot NOD + c, \tag{1}$$

where Dfactor is the normalized correction factor describing the temporal degradation. NOD is the number of elapsed days since January 1st, 1900, starting with 1. a, b, and c are the fitting coefficients of the polynomial function based on the near-infrared radiance of the pseudo-invariant site, the detailed analysis can be found in Sect.4.1.

Line 253:

The second-order polynomial (Dfactor) fitted by the normalized coefficient was used in Eq. (2) to calibrate the instrument's degradation since 1 January 2007, as given by:

$$\text{Dfactor(NOD)} = 80.298 \times \left(\frac{NOD}{100000}\right)^2 - 70.123 \times \frac{NOD}{100000} + 16.142, \ (R^2 = 0.851), \tag{11}$$

where Dfactor is the degradation coefficient and "NOD" is the number of days since January 1st, 1900.

Minor comment 6: Line 217: "upscale the daily observations to monthly values" – This is confusing. The previous sentence emphasized the potential bias of upscaling instantaneous measurements to daily values.

Response: Thanks for the comment. The statement here is to illustrate that compared with the upscaling method using cos(SZA), extending the instantaneous SIF to the daily average using PAR has a lower potential bias. We have modified this sentence to be more understandable in the revised manuscript:

Line 224:

In previous studies, the global satellite-observed SIF was upscaled to a daily scale by using the diurnal cycle of the cosine of the solar zenith angle (cos[SZA]) to correct for day-length effects (Frankenberg et al., 2011; Zhang et al., 2018). These effects can cause large overestimates of SIF on cloudy days because the satellite-observed SIF data are only available on clear-sky days. **In this study, the downwelling PAR rather than cos(SZA) was used to compensate for the significant effects of diurnal weather changes due to cloud and atmospheric scattering (Hu et al., 2018) while upscaling the instantaneous SIF to monthly values.** The all-sky monthly averaged SIF (SIF_{mon}) can be determined using the PAR-based upscaling model, as follows:

$$\text{SIF}_{\text{mon}} = \begin{cases} \frac{\sum_{\text{mon}}^{M} \text{SIF}_{\text{ins}}}{\sum_{\text{mon}}^{M} \text{PAR}_{\text{ins}} \times \text{EVI}_{\text{ins}}} \times \text{PAR}_{\text{mon}} \times \text{EVI}_{\text{mon}}, \text{if } \text{EVI}_{\text{mon}} > 0.2 \\ \\ \frac{\sum_{\text{mon}}^{M} \text{SIF}_{\text{ins}}}{\sum_{\text{mon}}^{M} \text{PAR}_{\text{ins}}} \times \text{PAR}_{\text{mon}}, \text{if } \text{EVI}_{\text{mon}} \leq 0.2 \end{cases}, \tag{10}$$

Minor comment 7: Line 233: Could you clarify what the "normalized coefficients" stand for?

Response:

Thanks for the comment. The "normalized coefficients" are calculated by dividing the NIR reflectance by the value of its fitting function (shown in Figure 3a) on the starting date (1 January 2007). This ensures that the second-order correction function (Dfactor), which is fitted based on the normalization coefficient, has a value of 1 on the starting date. We have to apologize that the previous Figure 3 (b) was wrongly depicted, which might be confusing, we have revised it in the latest version of our manuscript. In fact, there is only a multiplicative factor between the reflectivity and the normalization coefficients, and the distribution of the scatter points is exactly the same. We have added explanations to both the figure captions and the main text, and the revisions are as follows:

Line 240:
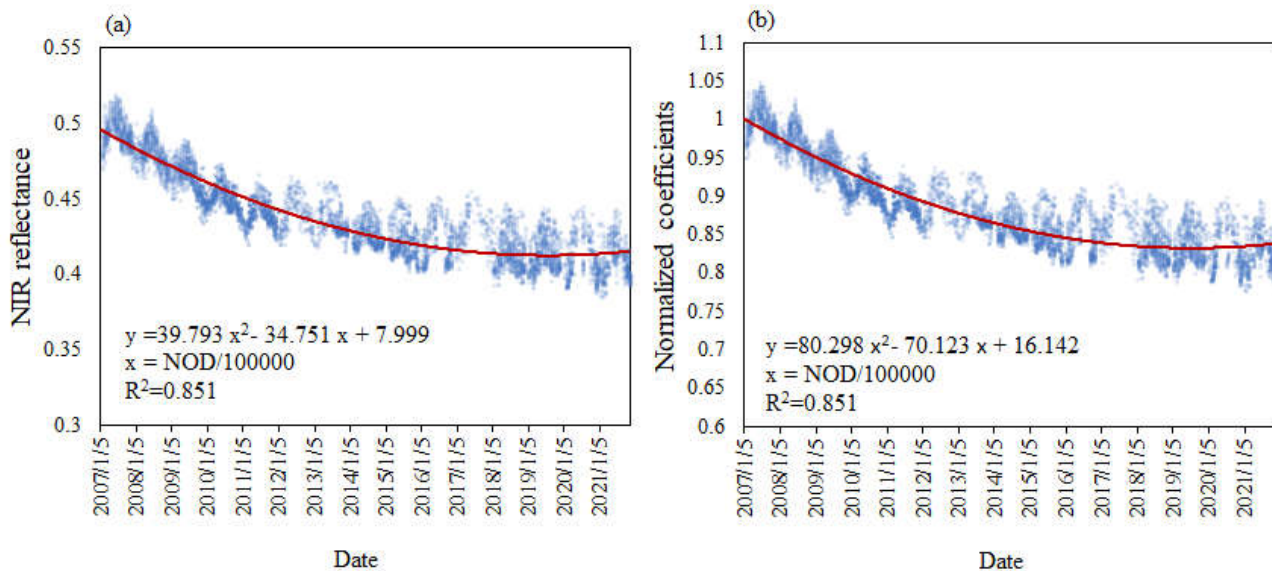
Figure 3. Temporal variation in the TOA reflectance at 758 nm at the calibration site (left) and the temporal correction coefficients used to compensate for the degradation of GOME-2A since 2007 (right). **The blue dots and red curves in (a) represent NIR reflectance and the fitted quadratic function. The normalized coefficients in (b) were calculated by dividing the NIR reflectance by the value of the quadratic function in (a) at the starting date (1 January 2007).** "NOD" in the degradation correction equation is the GOME-2A acquisition date since 2007, which equals the number of days from 1 January 1900.

A second-order polynomial was fitted to describe the temporal degradation in the reflectance signal of GOME-2A. Figure 3 a illustrates the temporal variation in TOA reflectance at 758 nm at the calibration site. Significant and continuous degradation can be observed; however, this nonlinear trend could be accurately captured by a quadratic polynomial function with a determination coefficient (R^2) of 0.851. These results

indicated that, overall, the GOME-2A instrument degraded by 16.21 % from 2007 to 2021. This temporal degradation was considered spectrally constant in the narrow fitting window of SIF retrieval (735–758 nm).

By dividing the NIR reflectance by the value of the fitted function at the starting date (1 January 2007), we obtain the normalized temporal correction coefficients, as shown in Figure 3 b. The second-order polynomial (Dfactor) fitted by the normalized coefficient was used in Eq. (2) to calibrate the instrument's degradation since 1 January 2007, as given by:

$$\text{Dfactor(NOD)} = 80.298 \times \left(\frac{\text{NOD}}{100000}\right)^2 - 70.123 \times \frac{\text{NOD}}{100000} + 16.142, \ (R^2 = 0.851), \tag{11}$$

where Dfactor is the degradation coefficient and "NOD" is the number of days since January 1st, 1900.

Minor comment 8: Fig. 10: The two green colors are not very distinguishable visually. Also, comparison with other datasets in terms of the trend maps may be useful, e.g., which regions have significant increase/decrease, are they consistent among different datasets?

Response: Thanks for this comment, the color of the "increase" trend is changed to be more distinguishable as below:

Line 328:
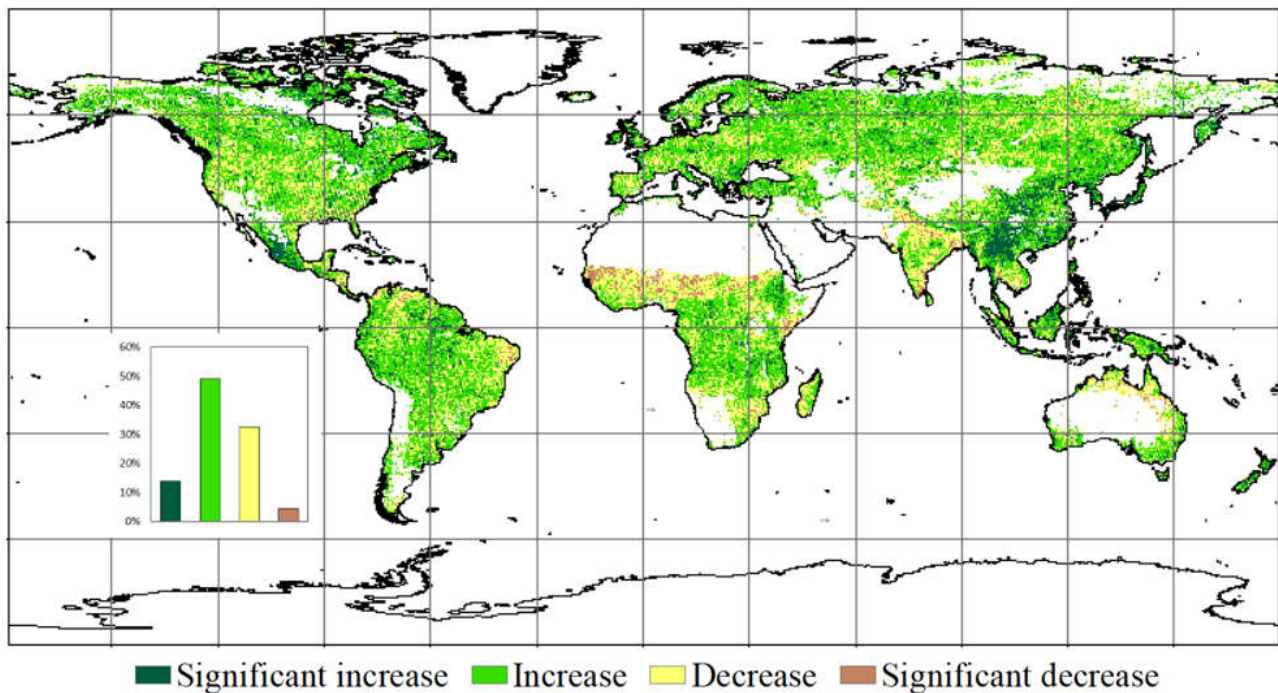
Figure 10. Map of trends in the annual average GOME-2A SIF for 2007–2021. The inset shows the percentage of areas characterized by four types of trends (significant increase: positive correlation with $p < 0.05$; increase: positive correlation with $p \geq 0.05$; decrease: negative correlation with $p \geq 0.05$; significant decrease: negative correlation with $p < 0.05$).

Besides, the trend maps of GPP, NDVI, NASA SIF, and OCO-2 SIF were analyzed in the revised manuscript as follows:

Line 332:
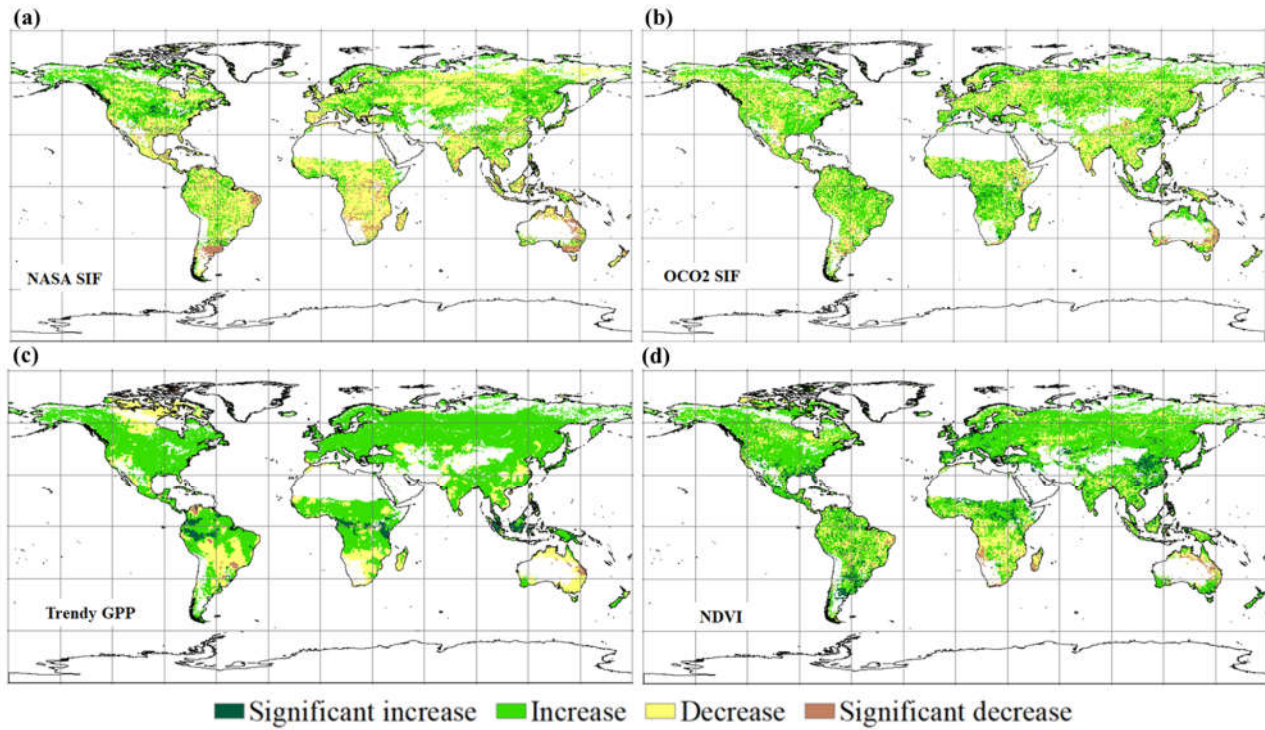
Figure 11. Map of trends in the annual average (a)NASA SIF for 2007–2018, (b) OCO-2 SIF for 2015–2021, as well as (c) Trendy GPP and (d) NDVI for 2007–2021. The colors represent four types of trends (significant increase: positive correlation with $p < 0.05$; increase: positive correlation with $p \geq 0.05$; decrease: negative correlation with $p \geq 0.05$; significant decrease: negative correlation with $p < 0.05$).

As shown in Figure 11, 57.11% of vegetation areas are facing a decline in NASA SIF. On the opposite, as seen from OCO-2 SIF, trendy GPP, and NDVI, vegetation is growing over a large area globally (>70%) from 2007 (or 2015) to 2021. The main inconsistency between NASA SIF and the other products occurs in central and southern Africa, eastern Europe, and southern North America, where NASA SIF declines and the others increase. In southeastern China, vegetation greenings were found by TCSIF, OCO-2 SIF, and NDVI, while an insignificant downward trend was shown by trendy GPP. Vegetation growth in southern North America, Europe, the Amazon rainforest, central Africa, and Southeast Asia was detected by all the products apart from NASA SIF.

Minor comment 9: Line 311: Please justify why the trend of annual maximum was selected for evaluation, not annual mean or annual minimum.

Response: Thanks for this comment. For comparison between different vegetation parameters (SIF, GPP, and NDVI), the annual maximum was selected because the annual maximum captures the period of peak vegetation activity, typically coinciding with the peak of the growing season. This allows us to focus on the most dynamic phase plant growth. Meanwhile, during the season with the highest SIF intensity, the effect from cloud and atmospheric scatter, as well as spatial noise caused by the retrieval algorithm are relatively low. On the contrary, during the period with the minimum SIF, the low global average signal is more susceptible to interference from noise and weather conditions, thus affecting the accuracy of the trend fitted. We have explained why and how we calculate the maximum value in the revised manuscript as shown below:

Line 441:

5.4 Interannual trends for the TCSIF, NDVI, and GPP products

We compared the interannual trend of TCSIF with that of GPP and NDVI. **Parameter values during the peak of the growing season were compared to show the most lush period of vegetation each year. After spatial averaging of monthly products, the yearly annual maximum values were calculated year by year.**

As evinced by Figure 16a–e, the global yearly maximum of TCSIF showed a trend of increasing SIF intensity, which was consistent with that of GPP and NDVI. The interannual fluctuation of TCSIF (0.16 %) slightly exceeded that of the GPP and NDVI products (<0.1 % yr^{-1}) during the 2007–2021 period, and likewise for 2007–2016. The interannual trend and associated uncertainty of each product are displayed in Figure 16f. Given that the timespan of Pmodel GPP stops at 2016, we selected the NDVI and TCSIF series from 2007 to 2016 for a fair comparison with Pmodel GPP, this is shown in the bottom half of Figure 16f. Evidently, there are deviations in the interannual growing trend of vegetation when inferred from different GPP products. For example, from 2007 to 2021, the interannual growth trend estimated by MODIS GPP (0.64 %) surpassed that of TRENDY GPP (0.44 %). Meanwhile, the interannual growth rate of TCSIF was close to that of MODIS GPP and Pmodel GPP in 2007–2021 and 2007–2016, respectively. Notably, when compared with the reflectance-based index NDVI, the trend of TCSIF was more similar to that of GPP in both periods examined, indicating that TCSIF was more capable of tracking GPP than NDVI.
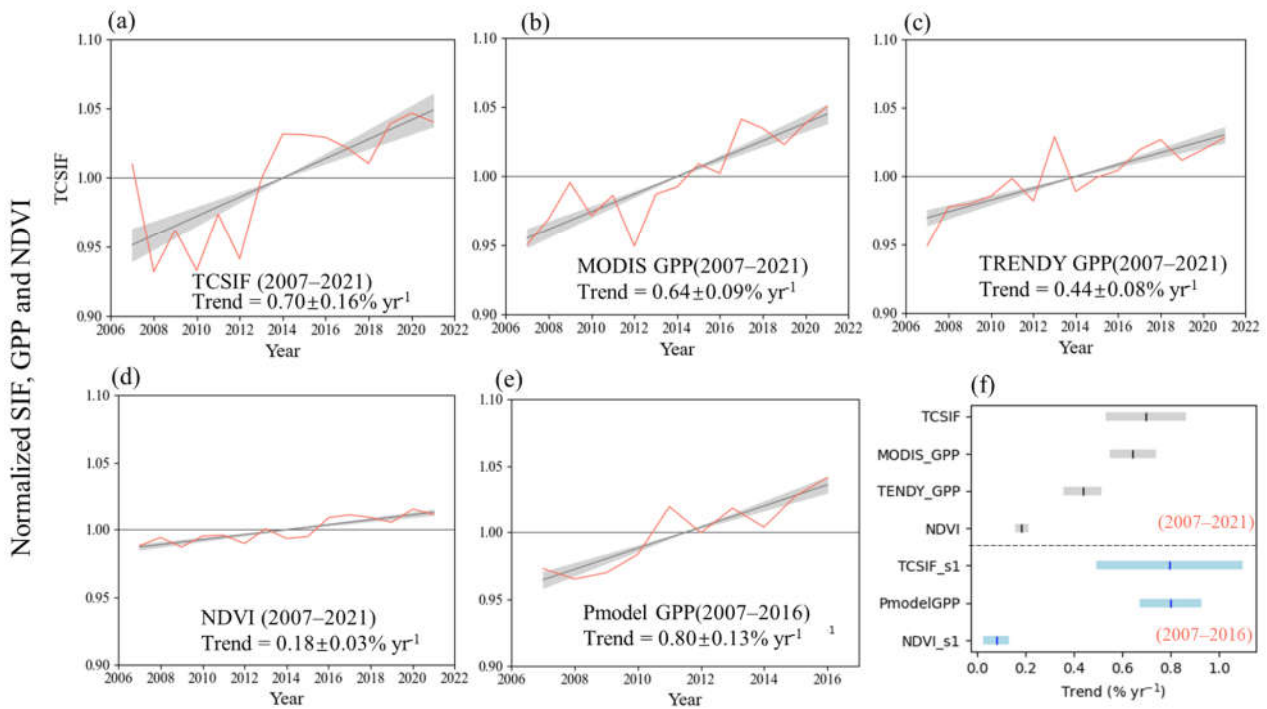
Figure 16. Comparison of temporal trends in the yearly maximum from (a) TCSIF, (b) TRENDY GPP, (c) Pmodel GPP, (d) MODIS GPP, and (e) NDVI. All data shown are normalized to relative values (by dividing the mean). The shaded areas indicate the standard deviations and the gray lines represent the fitted lines which show the general trends. The interannual trends (shown by the gray or blue vertical short lines) of all the products and their uncertainties (shown by the blue or gray horizontal bars) are shown in (f). TCSIF_s1 and NDVI_s1 correspond to the TCSIF and NDVI series for 2007–2016.

For comparison between SIF products, both the annual maximum and the annual mean value are used in the previous manuscript. For consistency, the annual average was used for comparison between SIF products was used in the revised manuscript. The relative revisions are as follows:

Line 401:

The annual average values of TCSIF and other long-term SIF products were compared as well (Figure 15). Importantly, most of the long-term SIF products were in agreement, featuring an increasing trend of SIF from 2007 to 2018, except for NASA SIF and SIFTER(Figure 15a–e). Among the temporal corrected SIF products, the annual curves of TCSIF and LTSIFc* are generally consistent, while LTSIFc* gives a higher growing trend of 1.247% yr^{-1}, and the uncertainty of the growing trend of TCSIF(0.15 % yr^{-1}) is lower. A slightly decreasing trend of -0.08 % yr^{-1} characterized the SIFTER v2 product (Figure 15b), while the annual fluctuation of SIFTER v2 was clearly greatest among all the SIF products shown in Figure 15 (0.37 % yr^{-1}). The yearly trend according to TCSIF (1.06 % yr^{-1}) is close to the results from OCO-2 SIF from 2015 to 2021 (1.23% yr^{-1}, Figure 15f), while GOSIF shows a lower growing trend of 0.50% yr^{-1} during the same period. Compared to GOSIF, which was derived from OCO-2 SIF using a machine learning method, TCSIF is even

more consistent with OCO-2 SIF, suggesting the flaws of machine learning methods in maintaining the temporal trend of the original SIF products.
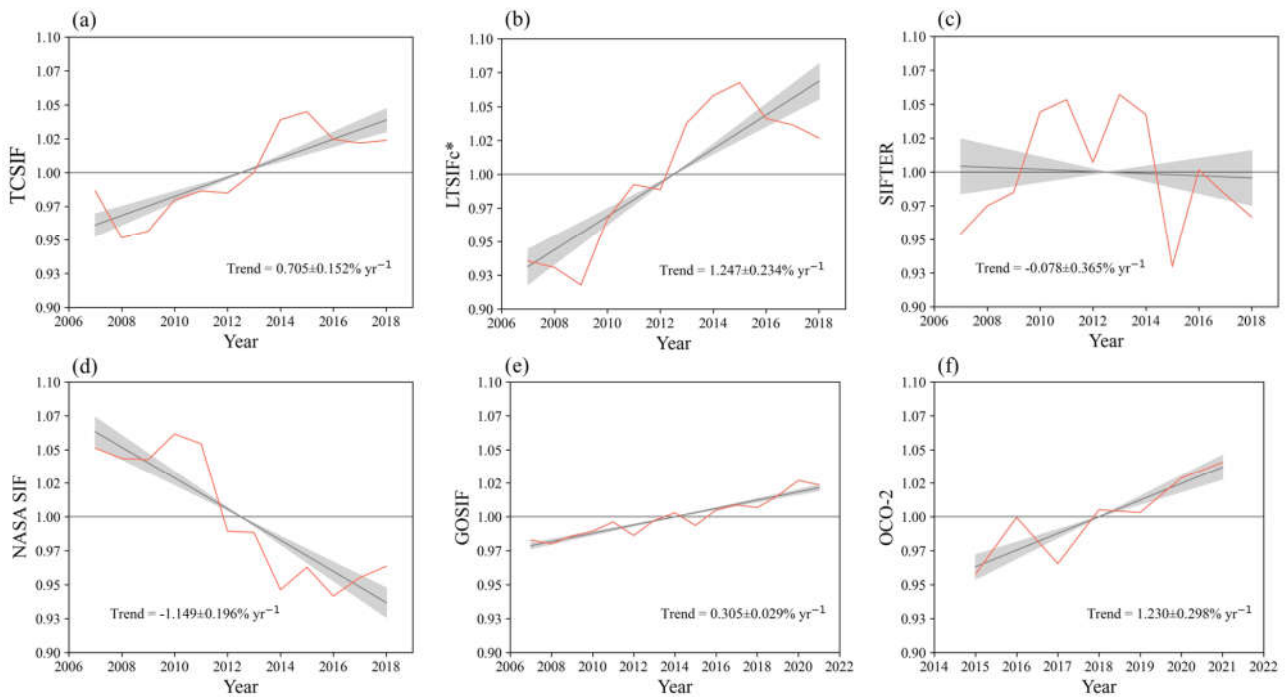
Figure 15. Comparison of temporal trends in the annual SIF average from (a) TCSIF, (b) LT_SIFc*, (c) SIFTER v2, (d) NASA SIF during 2007–2018, as well as (e) GOSIF during 2007–2021, and (f) OCO-2 SIF during 2015–2021. All data shown are normalized to relative values (by dividing the mean). The shaded areas indicated the standard deviations.

The large interannual fluctuation of SIFTER may be caused by the fact that its correction factor is seasonally based. No continuous correction functions were applied by SIFTER, which runs counter to the sensor's general pattern of temporal decay. (Lyapustin et al., 2014; Wang et al., 2012). In stark contrast, the least amount of interannual fluctuation was found in the GOSIF product. A neural network model was used for the spatiotemporal degradation of the GOSIF product, enabling GOSIF to inherit the time-stable signal from MODIS reflectance. However, this neural network model has been criticized for relying too much on training data such as reflectance data, and overlooking valuable information in the original observations (Ma et al., 2020). In the years not covered by the original OCO-2 SIF, the spatial distribution of GOSIF depends almost entirely on other input parameters of the data-driven model; hence, it cannot reliably capture the long-term temporal trend of SIF.

The LT_SIFc* product uses weak SIF signals over the Sahara Desert to fit the temporal decay pattern of the sensor, which can quickly generate corrected SIF products based on the monthly global maps provided by NASA SIF. Nevertheless, the method is not rigorous enough, since the sensor's degradation does not alter the SIF retrievals in a linear way. The post-processing steps, such as the zero-offset correction and quality-

filtering procedures, will influence the distribution of global-gridded SIF products, leading to uncertainties arising in the correction function. Besides that, a large proportion of noise signals accompany the weak SIF signals over desert targets, thus restricting the fitting accuracy of the corrective function. Meanwhile, LTSIF_c* is obtained by fusing three SIF products using the cumulative distribution frequency (CDF)-matching approach. Accordingly, the spatiotemporal distribution of the original SIF signal may be forced to change due to adjustments in the distribution frequency of each separate product. In this study, we corrected the degradation in radiance spectra rather than SIF by using pseudo-invariant pixels over the Sahara Desert, which should provide a more reliable method.

To take advantage of SIF's ability to quickly capture changes in GPP, the temporal resolution of long-term SIF products is supposed to be higher than 1 month and even a few days (Zhang et al., 2014; Zhang et al., 2016; Porcar-Castell et al., 2014). However, LT_SIFc* cannot meet those temporal resolution requirements constrained by the original SIF products. By contrast, the shorter, repeating cycle of GOME-2 was fully utilized in this study. Our work provides global daily level-2 SIF products that encompass the world's terrestrial area, which will greatly improve the application ability of global SIF products for monitoring global vegetation dynamics.

Minor comment 10: Fig. 12: it is also worth noting that the year-to-year variations are very different among different SIF products. Any idea why? Could you also add NASA SIF here to see if TCSIF has consistent year-to-year variations with NASA SIF?

Response: Thanks for this comment. It is true that we can see different year-to-year variations for different products, even though they are generated using the same sensor. Although all rely on GOME-2A measurements, the year-to-year variations shown by NASA SIF, TCSIF, and SIFTER are not always consistent. The discrepancy can be caused by the difference in a retrieval algorithm, post-processing method, and temporal correction method. For example, different retrieval model was used for TCSIF (SVD linear model) and NASA SIF (PCA non-linear model), and different temporal correction methods were applied for TCSIF (using daily correction factors) and SIFTER (using seasonal correction factors). According to minor comment 9, annual averages were selected for all the comparisons between SIF products. Besides, the interannual variation of NASA SIF was also added in the revised manuscript. The comparison of different SIF products as well as the analysis for the discrepancy were shown in the discussion (Sec. 5.3) in the revised manuscript. Detailed results are shown in **minor comment 9**.

Comparison using annual averages demonstrates better consistency in inter-annual fluctuations between TCSIF and other products. Especially, the interannual variation given by the annual mean of LTSIFc* shows a clearer trend ($1.25 \pm 0.23\%$ yr^{-1}) compared to that fitted by the annual maximum in the

previous version of the manuscript (0.21 $\pm$0.17% yr^{-1}). Meanwhile, the general conclusion was similar to that we derived in the previous version of the manuscript. For example, NASA SIF intensity declined from 2007 to 2018, and SIFTER shows a near-constant interannual trend with large yearly fluctuation, while overall increasing trends are captured by other SIF products.

Editorial suggestions:

Thanks for the advice, the expressions have been corrected as follows:

Line 41: "Given" -> "Given that"

Given that its global coverage capability starts from 2007, the GOME-2 satellite-based SIF dataset has been the most widely used for global monitoring of GPP, crop yield, drought, vegetation phenology, etc.

Line 52: "Forest" -> "forests"

For example, Yang et al. (2018) reported the SIF emission of the Amazon **forest** decreased during the 2015/2016 El Niño event when analyzed using the GOME-2 SIF data by Joiner et al. (2016), which is in conflict with the increase of the enhanced vegetation index (EVI) and downward solar shortwave radiation.

Line 116: "expansion" -> "extrapolation"

Line 122:

The GOSIF product (https://globalecology.unh.edu/data/GOSIF.html) is the spatiotemporal **extrapolation** product based on the global neural network model and OCO-2 SIF V8r product, with a spatial resolution of 0.05° and a temporal resolution of 8 days.

Bacour, C., Briottet, X., Bréon, F.-M., Viallefont-Robinet, F., and Bouvet, M.: Revisiting Pseudo Invariant Calibration Sites (PICS) Over Sand Deserts for Vicarious Calibration of Optical Imagers at 20 km and 100 km Scales, Remote Sensing, 11, 1166, 2019.

Cosnefroy, H., Leroy, M., and Briottet, X.: Selection and characterization of Saharan and Arabian desert sites for the calibration of optical satellite sensors, Remote Sensing of Environment, 58, 101-114, https://doi.org/10.1016/0034-4257(95)00211-1, 1996.